# Structure of the *Dietzia* Mrp complex reveals molecular mechanism of this giant bacterial sodium-proton pump (Supplementary Material)

Bin Li, Kaiduan Zhang, Yong Nie, Xianping Wang, Yan Zhao, Xuejun C. Zhang, and Xiaolei Wu

## Discussions

### *Why does a $Na^+/H^+$ exchanger need multiple subunits?*

The Mrp complex is the most complexed $Na^+/H^+$ exchanger known to date (1-3). In this PMF-driven secondary active transporter, protons constitute the driving substance, with sodium ions representing the substrate. Therefore, the energy released by proton transport must be large enough to compensate the free-energy gain by $Na^+$. The more protons are transported, the faster the transporter may work. This antiport activity enables the host cell to tolerate high salt concentration in its environment (4). In certain alkaliphilic bacteria, the Mrp complex is also responsible for proton uptake (5, 6), and thus the electrostatic component of PMF is the most probable energy source for such transporters (Fig. S9). In this case, a significant portion of the electrostatic energy from the proton transport is used to overcome the steep $\Delta$pH gradient, with the $Na^+$ efflux presumably playing an auxiliary role in the functional cycle of the transporter. A previous study showed that in these alkaliphilic bacteria (*e.g. B. pseudofirmus* OF4), the membrane potential ($\Delta\Psi$) is as strong as negative 180 mV (compared to –135 mV in neutralophilic bacteria such as *E. coli*), which is established mainly by ATP-driven $Na^+$ pumps (4). Thus, we



www.pnas.org/cgi/doi/10.1073/pnas.2006276117

estimate that the stoichiometry ratio of $H^+$: $Na^+$ must be higher than 4:1 to maintain the transport process in the desired direction (see below). Such a high ratio would be difficult (if not impossible) to achieve with simpler, canonical $Na^+/H^+$ exchangers (*e.g.* NhaA of a 2:1 stoichiometry ratio). Thus, the multi-subunit Mrp represents a thermodynamic solution to such challenge.

### *How many protons are needed to drive Mrp?*

If it is assumed that n protons are required to exchange for one $Na^+$ ion, then for alkaliphilic bacteria *B. pseudofirmus* OF4, the environmental pH can reach 10.5 and the cytosol pH is maintained at 8.3, giving a $\Delta$pH of 2.2 (4). To be imported, each proton needs to overcome the energy uphill of $2.3RT\Delta pH$. In the same process, each proton is driven by electrostatic energy of the membrane potential ($\Delta\Psi$), *i.e.* $FV_m$ (where $V_m \equiv |\Delta\Psi|$). Similarly, one $Na^+$ ion will be exported against a 10-fold concentration gradient ($\Delta$pNa =1) (7) as well as the membrane potential $\Delta\Psi$.

For the Mrp function cycle to proceed in the right direction, the driving energy from the PMF must be larger than the resistance of sodium ions.

$$n\,(FV_m - 2.3RT\Delta pH) > (FV_m + 2.3RT\Delta pNa)$$

Thus,

$$V_m > (2.3RT/F)\,(2.2n+1)/(n-1)$$

where $2.3RT/F \approx 59$ mV. For *B. pseudofirmus* OF4, the membrane potential is approx. –180 mV (4). Therefore, the number of protons being imported in order to exchange for a $Na^+$ ion must be larger than 4.

In case of alkaliphilic bacteria, the transporter in its $C_{out}$ state must be able to attract protons from the peripheral space with high affinity (*i.e.* high

$pK_a$). In contrast, the transporter must be able to release the protons to the cytosol, which is of relative low pH (higher proton concentration), with low affinity (*i.e.* low $pK_a$). Therefore, the (final) $pK_a$ value in the $C_{in}$ state is likely to be lower than that in the $C_{out}$ state. The differential binding energy $\Delta G_D(H^+)$ ($\equiv -2.3n\ RT\Delta pK_a > 0$) must be compensated by the electrostatic energy during the $C_{out}$-to-$C_{in}$ transition. $\Delta G_D(H^+)$ is a characteristic parameter of the transporter which does not change with the environmental pH (8).

### *Comparison of DqMrp with AfMrp*

During the revision of our manuscript, Steiner and Sazanov reported the structure of Group-I Mrp complex from *Anoxybacillus flavithermus* (AfMrp) (9). The overall structure of AfMrp is similar to our DqMrp complex (Fig. S13), and many of the structural descriptions are the same for both Mrp complexes. A few differences are, however, worth of discussions. First, in contrast to the six subunits in DqMrp, the AfMrp complex contains seven subunits. In particular, the MrpA subunit of DqMrp is separated into MrpA and MrpB in AfMrp. Nevertheless, this difference in primary structures does not cause major reorganization in the 3D structures of the complexes. Therefore, the structures of AfMrp and DqMrp are representatives of Group-I and -II of the Mrp family, respectively.

Secondly, the AfMrp structure was determined in an elongated dimer form, with the MrpE subunit serving as the dimerization interface. Since MrpE of DqMrp lacks of the two N-terminal transmembrane helices (Fig. S13) which are required for the dimerization of AfMrp by using domain-swapping, our DqMrp complex is unable to adapt the same dimer conformation. Therefore, the dimerization is unlikely to be a general requirement for the function of Mrp complexes.

Thirdly, in the AfMrp complex, a highly negatively charged cavity is reported to be located between the MrpA and MrpF subunits, and this cavity is further suggested to be part of the $Na^+$-transport path. However, there is no significant cavity observed in corresponding position in our DqMrp complex; in particular, this region lacks of a cluster of acidic residues. Furthermore, results of our NaCl-resistance assay on the mutations at $D36^{F2}$ in DqMrpF (corresponding to D35 in AfMrpF) suggest that the precise location of the only acidic residue in this region, $D36^{F2}$, is not critical for the transport function (Fig. 4). Therefore, our DqMrp complex seems to use a $Na^+$-transport path distinct from the one proposed for AfMrp.

## Supplemental Figures

### *Figure S1. Sequence alignments of individual Mrp subunits from different species and their counterparts in the MBH*

Sequence alignments of homologous MrpA proteins: (A) MrpA; (B) MrpD; (C) MrpC; (D) MrpE; (E) MrpG; (F) MrpE. Conserved residues are highlighted in colors, blue for absolute identity and green for those of conserved properties. Secondary structures observed in the *Dietzia* sp. DQ12-45-1b Mrp complex are marked on the top; missing parts are shown as dash lines. The positions of our mutations are marked with circles: red circles represent loss-of-function mutants, and green circles represent wild-type-like mutants. The mutations summarized in Table S2 are marked with triangles: red triangles represent loss-of-function mutants, and green triangles represent wild-type-like mutants. Protein sequence sources are Dq, *Dietzia* sp. DQ12-45-1b; Rm, *Rhizobium meliloti* (strain 1021); Xc, *Xanthomonas campestris pv. campestris* (strain B100); At, *Agrobacterium tumefaciens*; Ba, *Brucella abortus biovar 1* (strain 9-941); Pa, *Pseudomonas aeruginosa* (strain ymp); Bs, *Bacillus subtilis* (strain 168); Bp, *Bacillus pseudofirmus* OF4; Sa, *Staphylococcus aureus*; Dh, *Desulfitobacterium hafniense* (strain Y51); Hz, *Halomonas zhaodongensis*; Li, *listeria innocua* atcc 33091; Pf, *Pyrococcus furiosus*. The sequences were alignment using the Clustal Omega program (10). (G). Mapping of conservation property of the sequence alignment on to the 3D structure of the Mrp complex.

A

MrpA

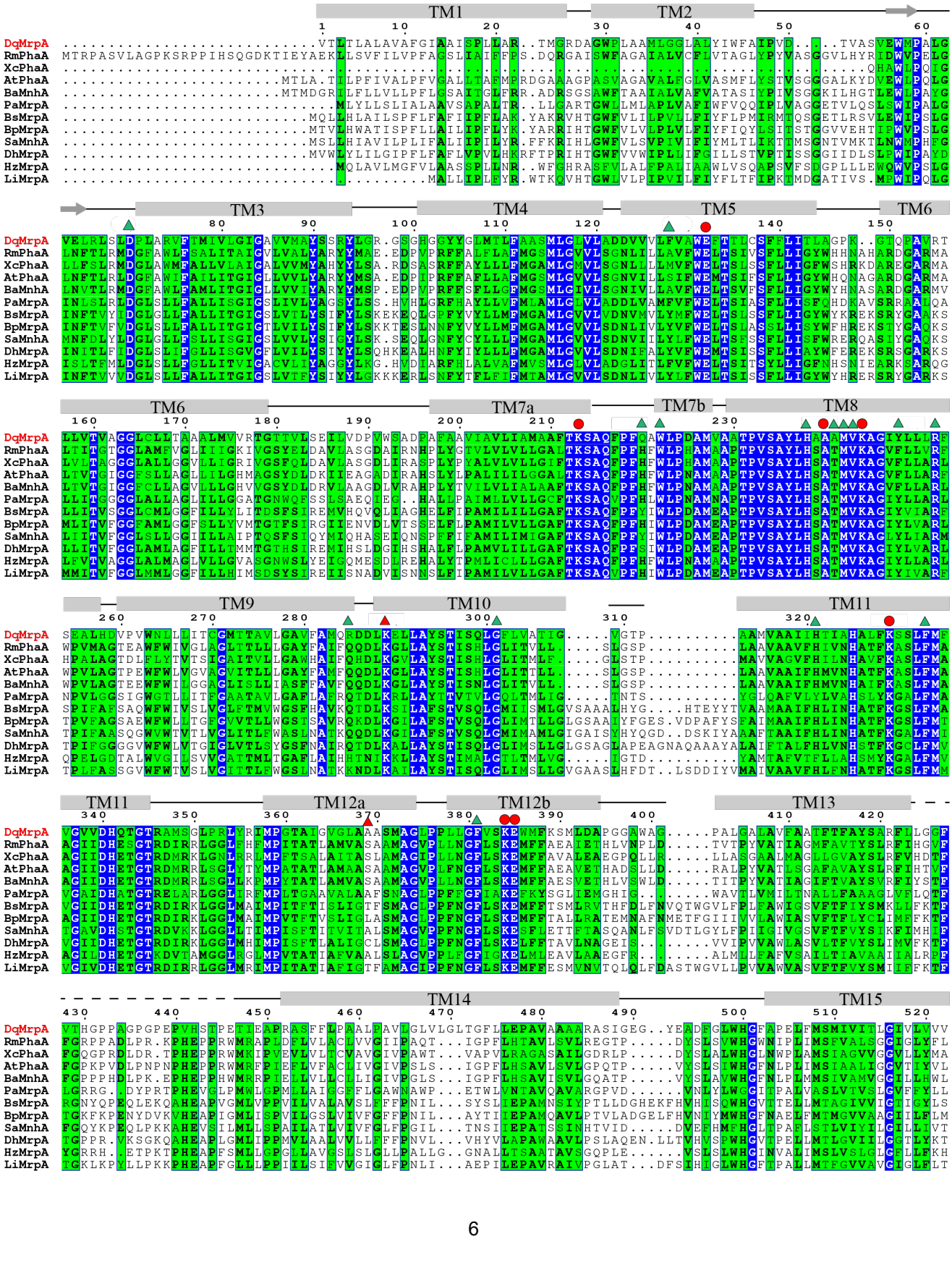
TM1
TM2
TM3
TM4
TM5
TM6
TM7a
TM7b
TM8
TM9
TM10
TM11
TM12a
TM12b
TM13
TM14
TM15
DqMrpA
RmPhaA
XcPhaA
AtPhaA
BaMnhA
PaMrpA
BsMrpA
BpMrpA
SaMnhA
DhMrpA
HzMrpA
LiMrpA

MrpA

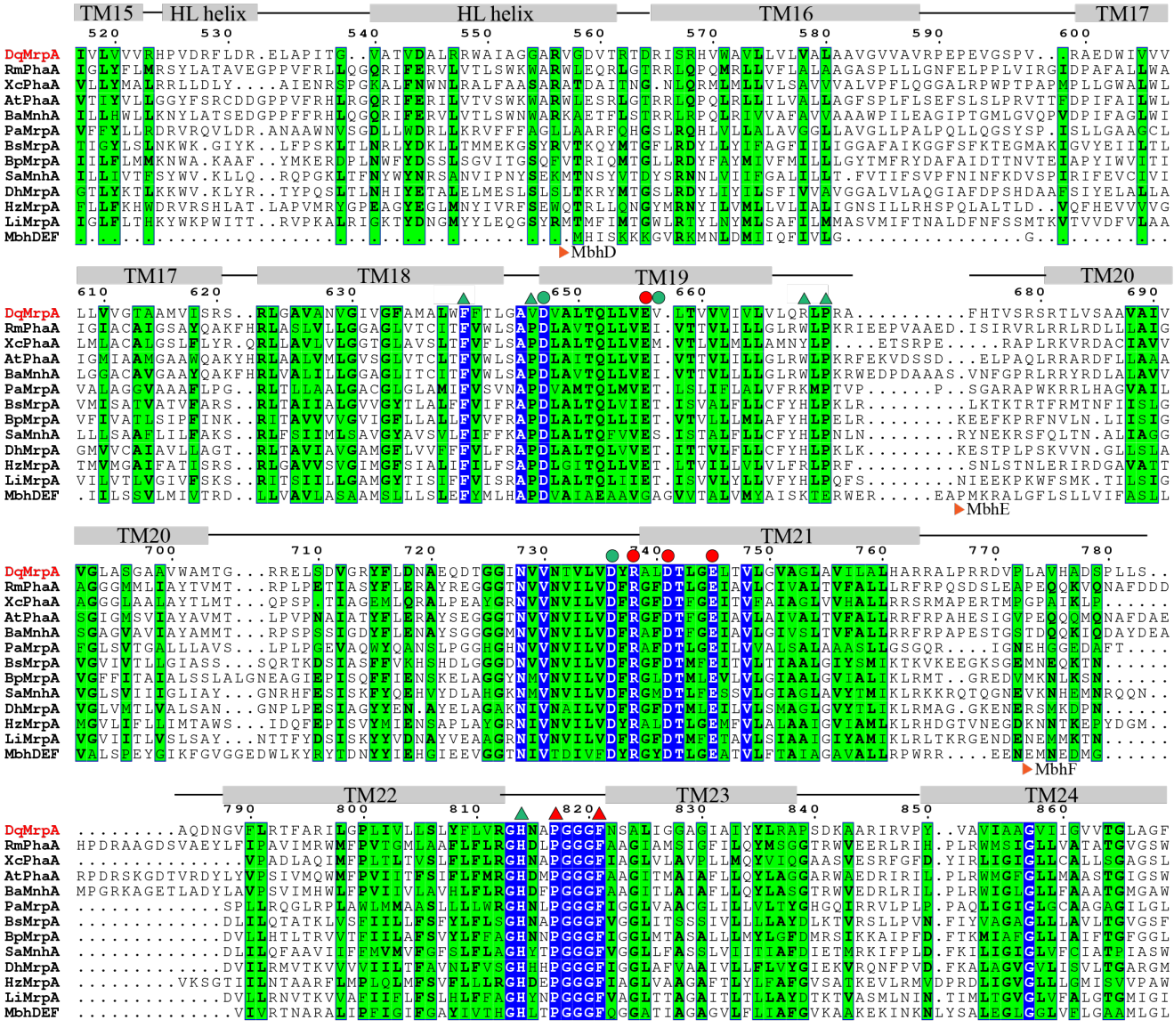
TM15
HL helix
HL helix
TM16
TM17
TM18
TM19
TM20
TM21
TM22
TM23
TM24
TM25
MbhD
MbhE
MbhF
DqMrpA
RmPhaA
XcPhaA
AtPhaA
BaMnhA
PaMrpA
BsMrpA
BpMrpA
SaMnhA
DhMrpA
HzMrpA
LiMrpA
MbhDEF

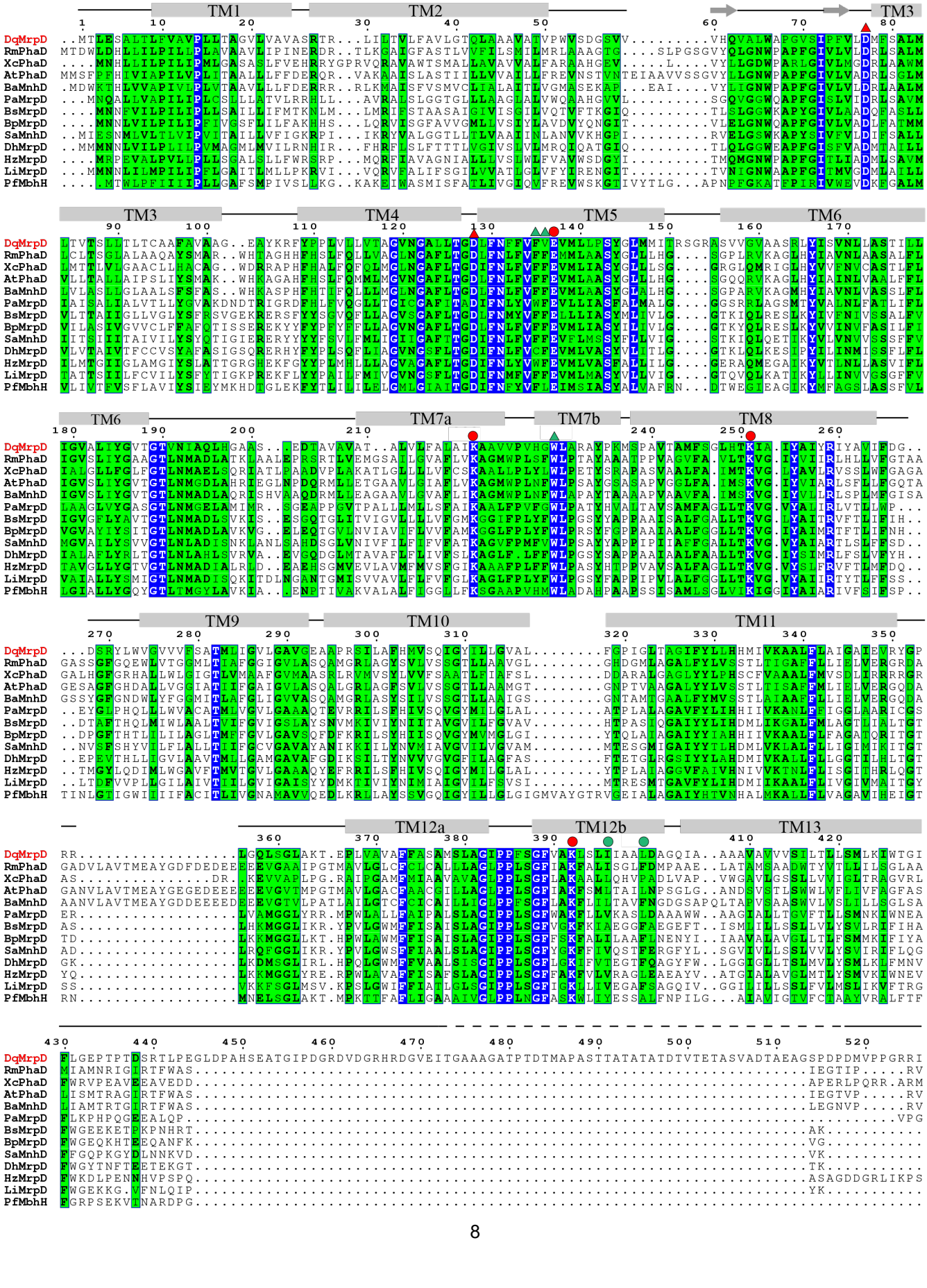
TM1
TM2
TM3
DqMrpD
RmPhaD
XcPhaD
AtPhaD
BaMnhD
PaMrpD
BsMrpD
BpMrpD
SaMnhD
DhMrpD
HzMrpD
LiMrpD
PfMbhH

## MrpD

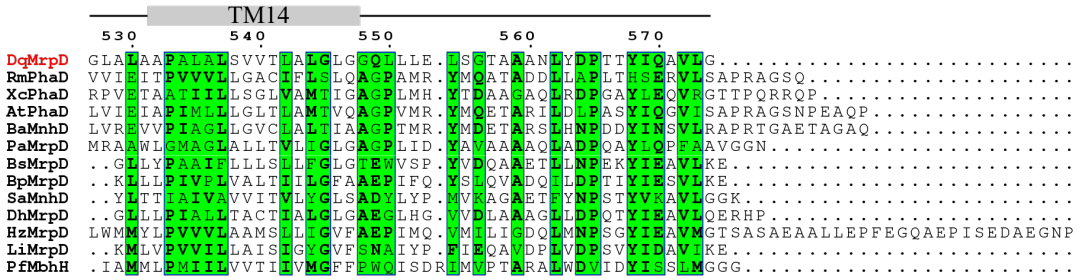


## MrpC

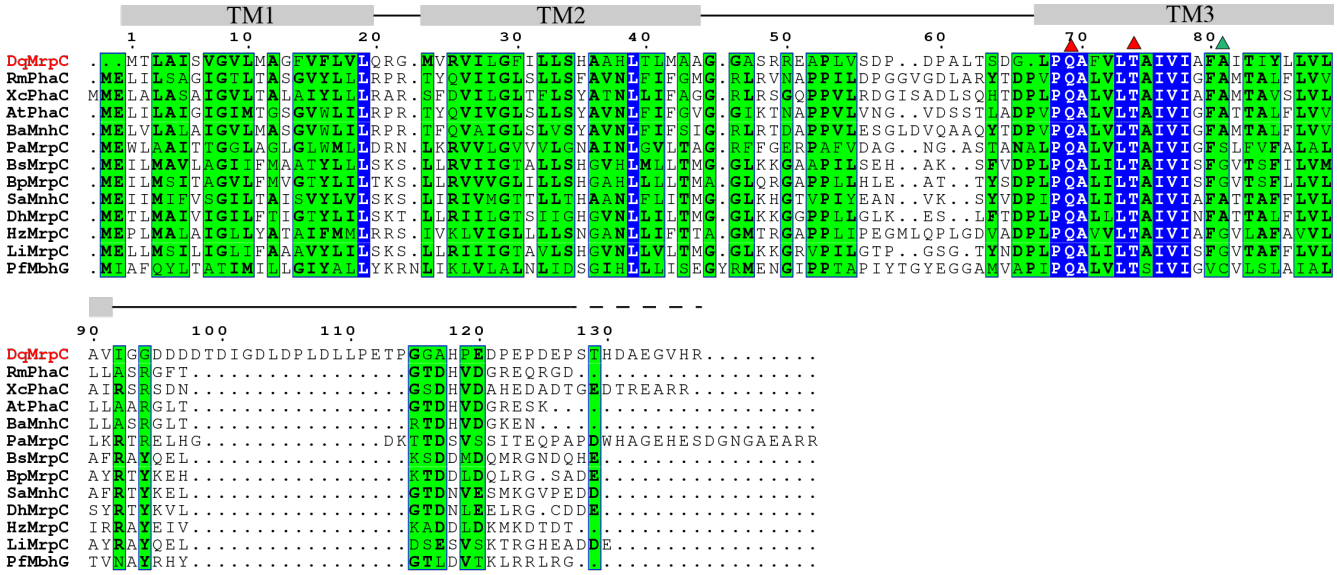


## MrpE

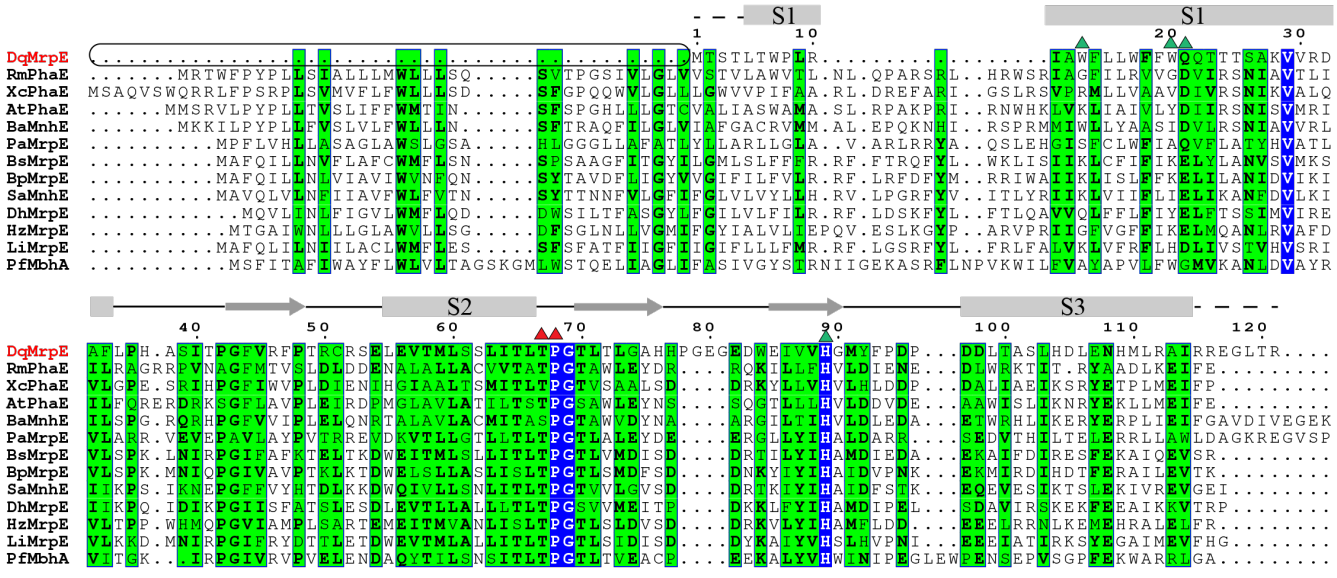

E

MrpF

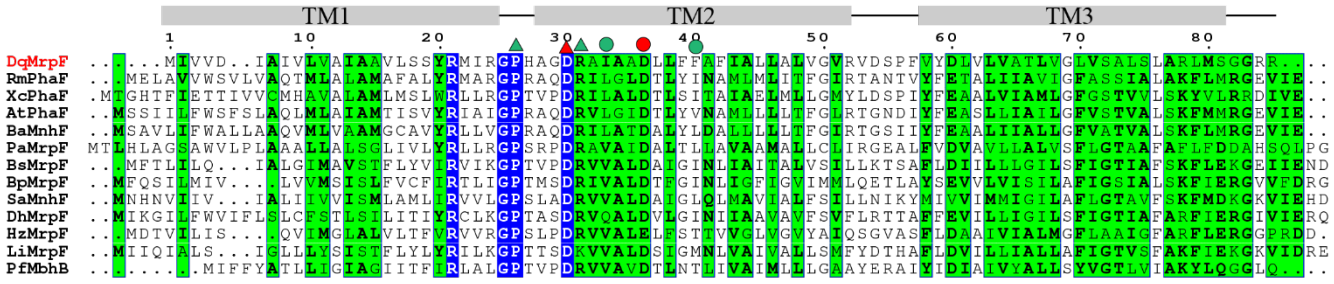


F

MrpG

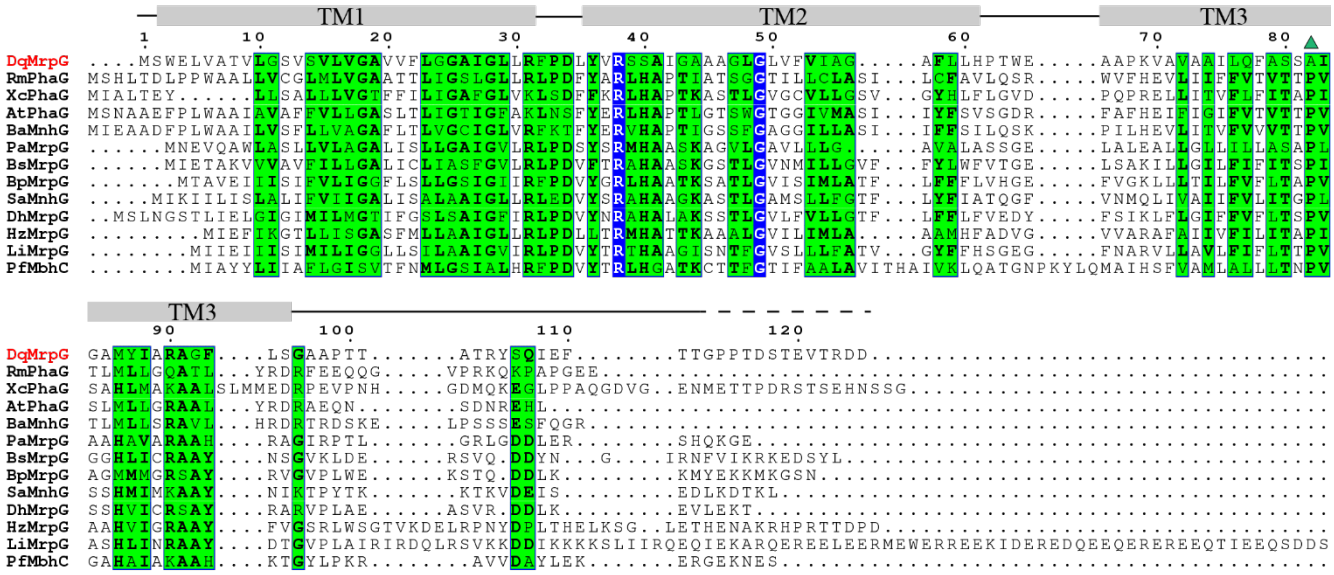


G

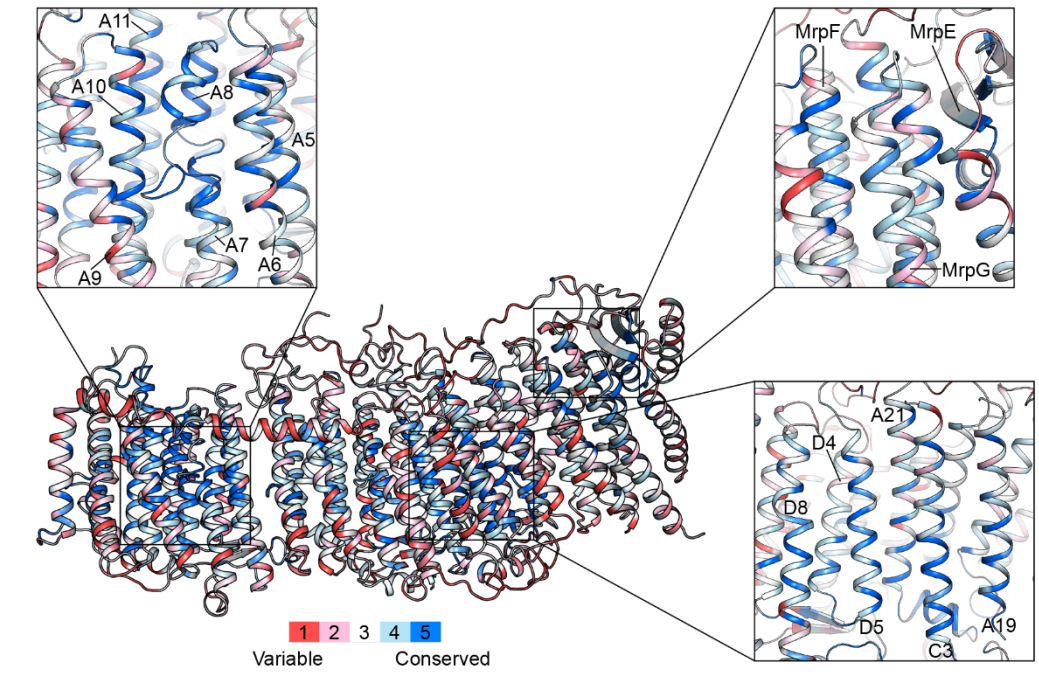

*Figure S2. Purification and cryo-EM of Dietzia sp. DQ12-45-1b Mrp complex*

(A). A representative size-exclusion chromatography trace of the purified Mrp complex solubilized with DDM.

(B). SDS-PAGE shows the presence of all six Mrp subunits as labeled on the right. Protein markers (PM in kDa) are labeled as shown on the left.

(C). Representative cryo-EM micrograph of Mrp particles.

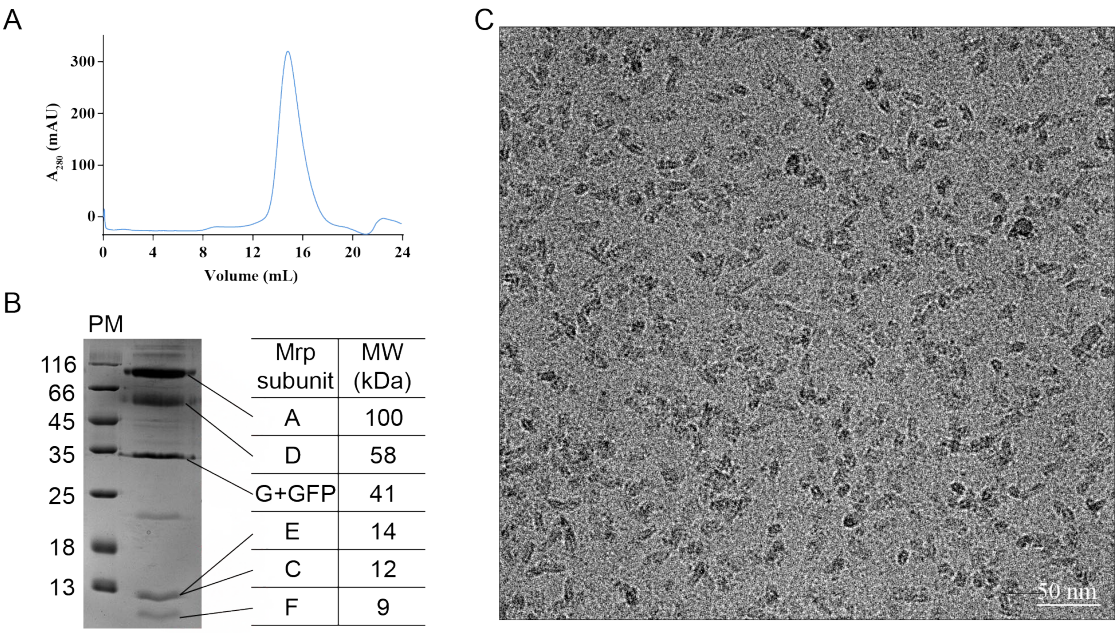

*Figure S3. Cryo-EM Analysis of Dietzia sp. DQ12-45-1b Mrp complex*

(A). The workflow of cryo-EM data processing. A total of 293,049 particles were selected using the Gautomatch software from 1,835 motion corrected micrographs. After removing detergent micelles and other false positives in several rounds of 2D classification, 137,082 particles were selected to generate the initial model.

(B). Angular distribution of all particles used in the final 3D reconstruction.

(C). The Fourier shell correlation (FSC) curve between partial 3D maps is shown in red. The FSC curve between the atomic model and the experimental map is shown in black. 3D maps are colored according to their local resolution, as determined by ResMap.

(D). Local resolution of the Mrp, The range of resolution is color-coded from the higher resolution blue (2.5 Å) to the lower resolution red (4.5 Å).

(E). Representation of the refined composite coordinate model, colored according to the B factors of the model atoms.

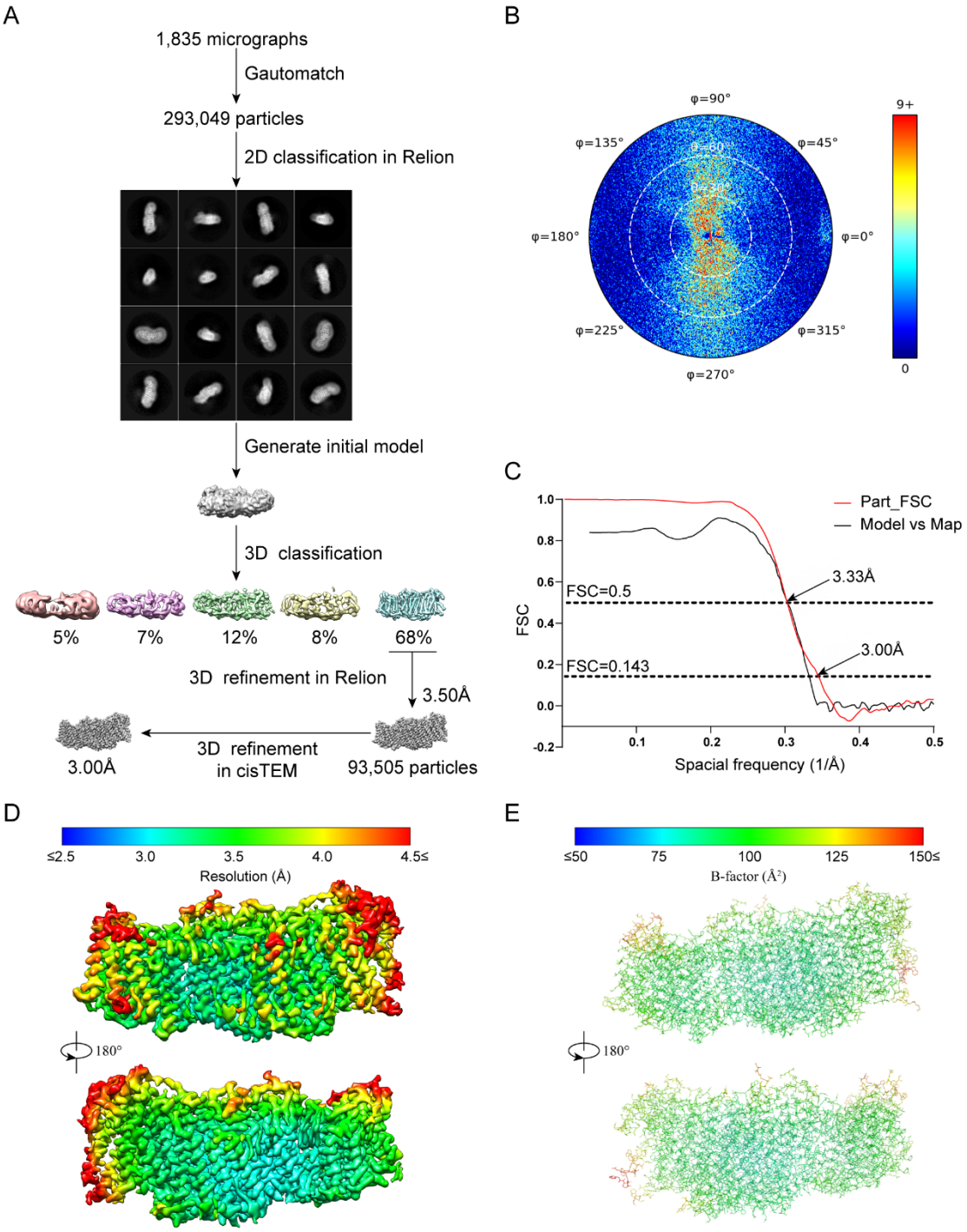
A
1,835 micrographs
Gautomatch
293,049 particles
2D classification in Relion
Generate initial model
3D classification
5%
7%
12%
8%
68%
3D refinement in Relion
3.50Å
3.00Å
3D refinement
in cisTEM
93,505 particles
B
φ=90°
φ=135°
φ=45°
φ=180°
φ=0°
φ=225°
φ=315°
φ=270°
θ=60°
θ=30°
9+
0
C
Part_FSC
Model vs Map
FSC=0.5
FSC=0.143
3.33Å
3.00Å
FSC
Spacial frequency (1/Å)
D
≤2.5
3.0
3.5
4.0
4.5≤
Resolution (Å)
180°
E
≤50
75
100
125
150≤
B-factor (Å²)
180°

*Figure S4. A gallery of EM density maps of representative transmembrane helixes of Mrp complex*

(A). Maps are superimposed with their corresponding atomic models in cartoon (main chains) and stick (side chains) presentations.

(B). Representative densities of lipid molecules are shown in their stick models.

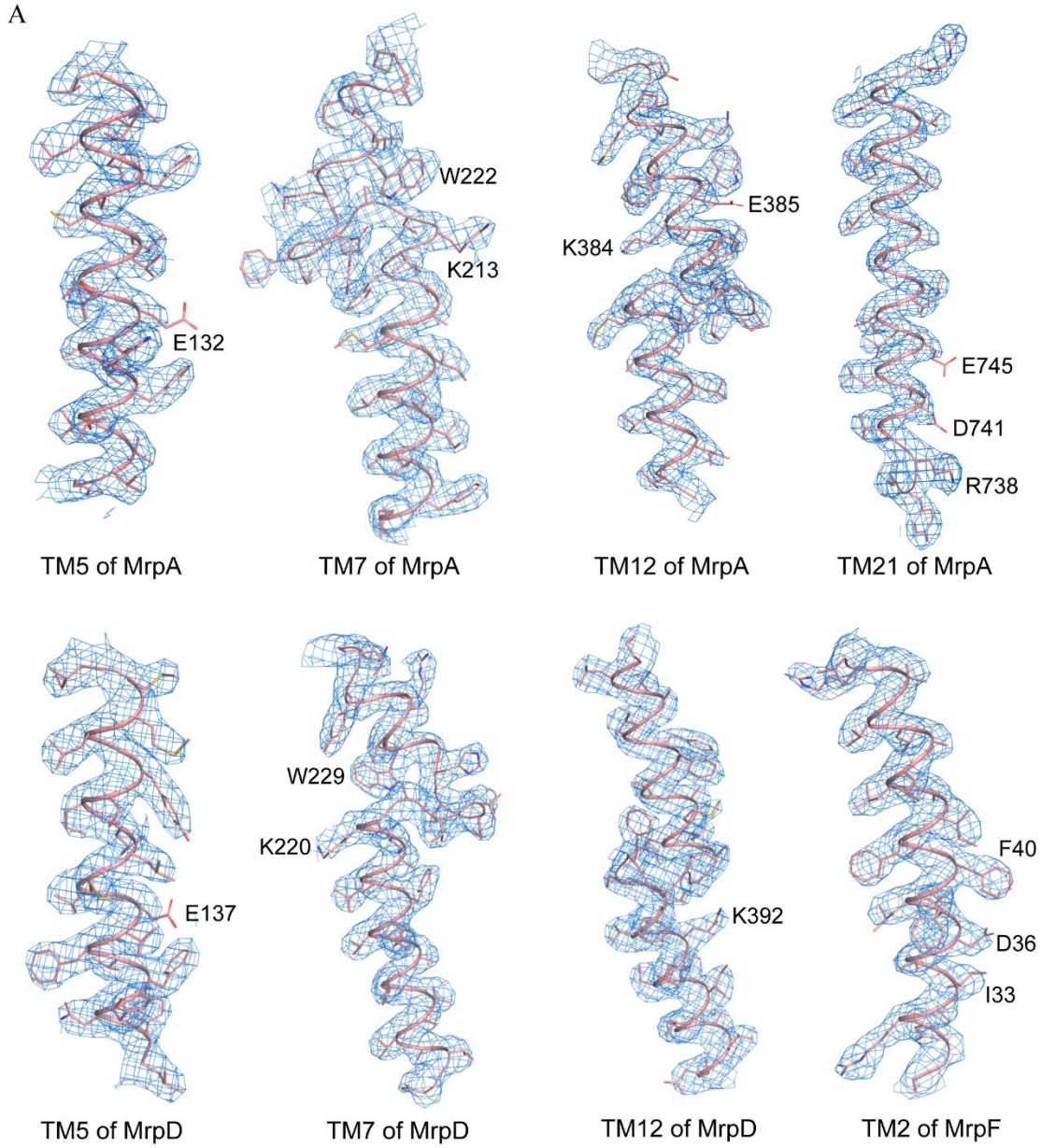

B

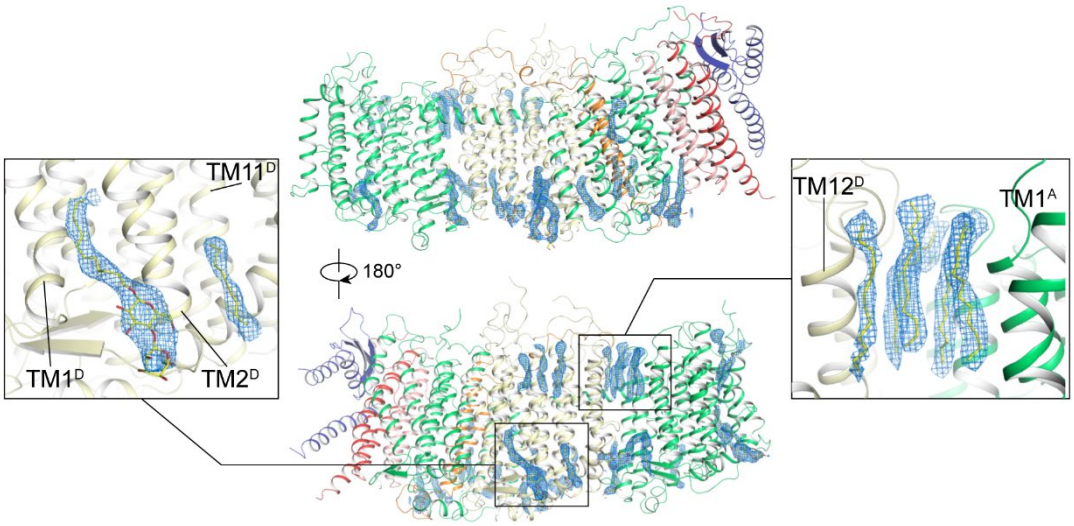

*Figure S5. Structural twist and constraint of Mrp complex*

(A). Structural twist within the Mrp complex viewed from different directions.

(B). The arrangement of TM helixes from different subunits along the central curve of the Mrp complex. Subunits are colored identical to (A).

(C). HL-helix and βH-belt (green) of the Mrp complex.

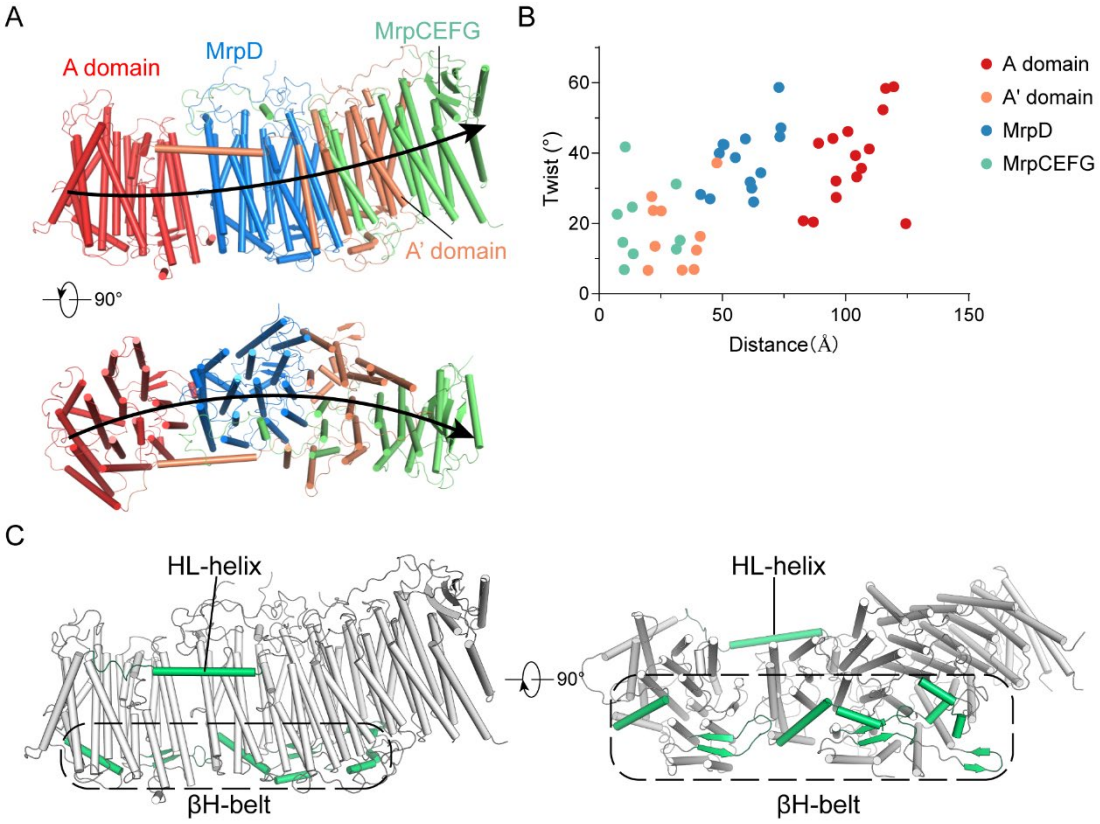

*Figure S6. Sequence alignments of individual Mrp subunits and their counterparts in the Complex I from different species*

(A). Sequence alignments of MrpA - A domain and its counterparts in the Complex I. Conserved residues in the central polar axis are marked with stars.

(B). Structural alignment of MrpA - A domain (green) and Nqo12 (grey, PDB ID: 4HEA). The conserved charged residues are shown as stick models.

(C). Structural alignment of MrpD (green) and Nqo14 (grey, PDB ID: 4HEA). The conserved charged residues are shown as stick models.

(D). Sequence alignments of MrpD and the counterparts in the Complex I and MBH. Conserved residues in the central polar axis are marked with stars.

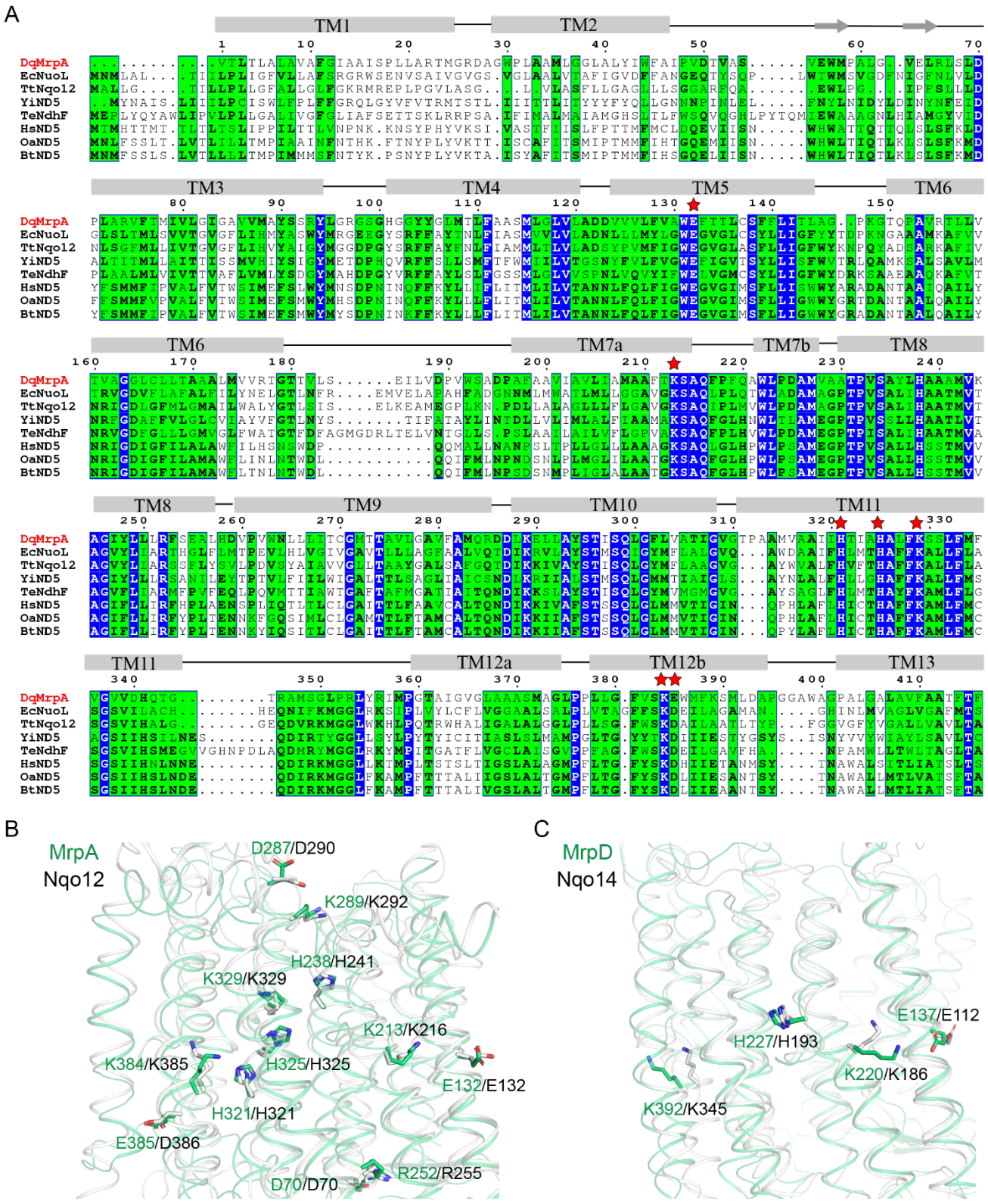
A
TM1
TM2
TM3
TM4
TM5
TM6
TM6
TM7a
TM7b
TM8
TM8
TM9
TM10
TM11
TM11
TM12a
TM12b
TM13
DqMrpA
EcNuoL
TtNqo12
YiND5
TeNdhF
HsND5
OaND5
BtND5
B
MrpA
Nqo12
D287/D290
K289/K292
H238/H241
K329/K329
K213/K216
K384/K385
H325/H325
E132/E132
H321/H321
E385/D386
D70/D70
R252/R255
C
MrpD
Nqo14
E137/E112
H227/H193
K220/K186
K392/K345

D

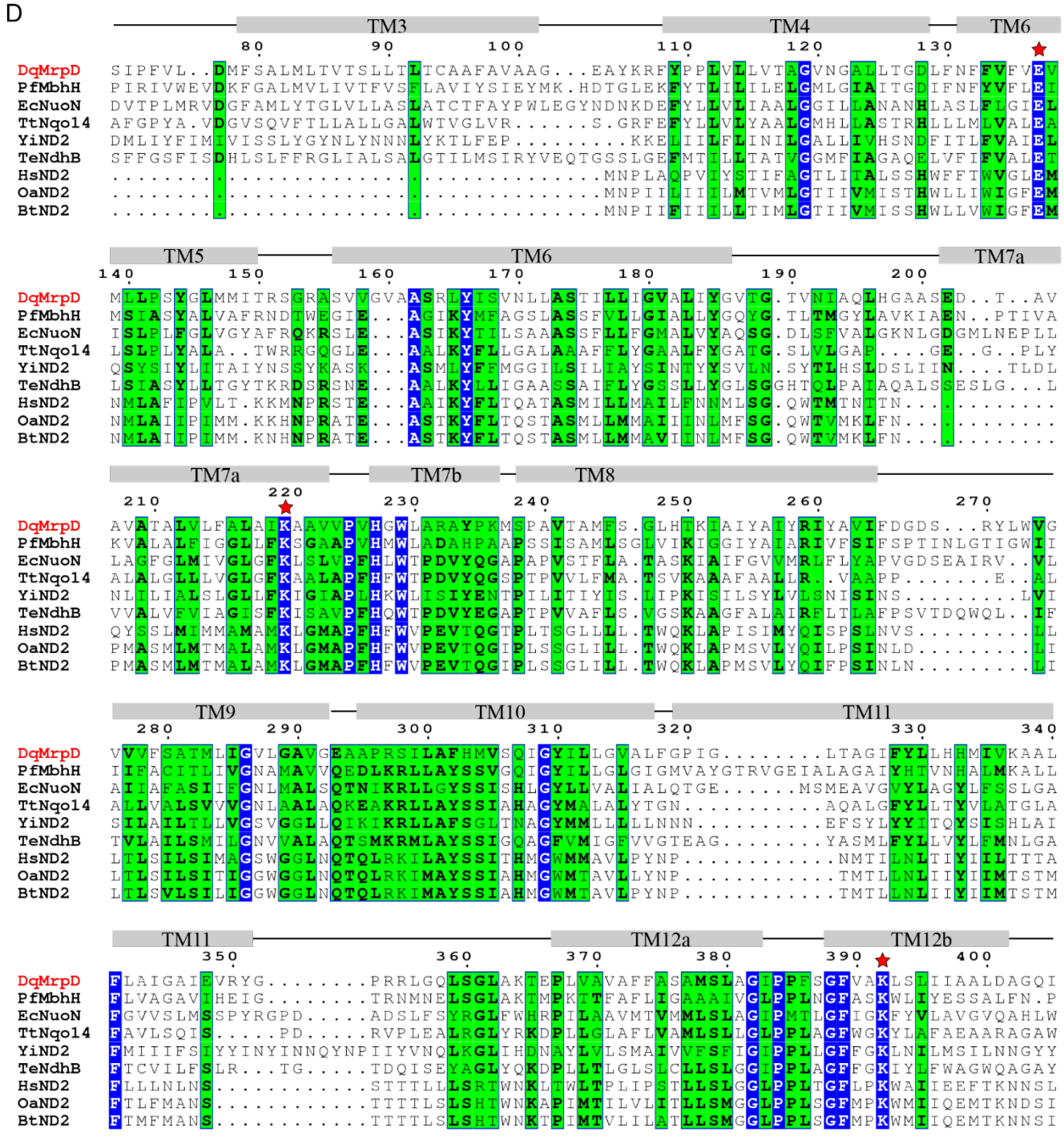
TM3
TM4
TM6
TM5
TM6
TM7a
TM7a
TM7b
TM8
TM9
TM10
TM11
TM11
TM12a
TM12b
DqMrpD
PfMbhH
EcNuoN
TtNqo14
YiND2
TeNdhB
HsND2
OaND2
BtND2

*Figure S7. Salt-resistance assay in E. coli KNabc cells*

(A). Colony formation on solid medium lacking NaCl.

(B). Colony formation on solid medium containing 200 mM NaCl.

(For completeness, certain results already shown in Fig. 4 are shown here again in their original form.)

*(Fig. S7A 1/2)*

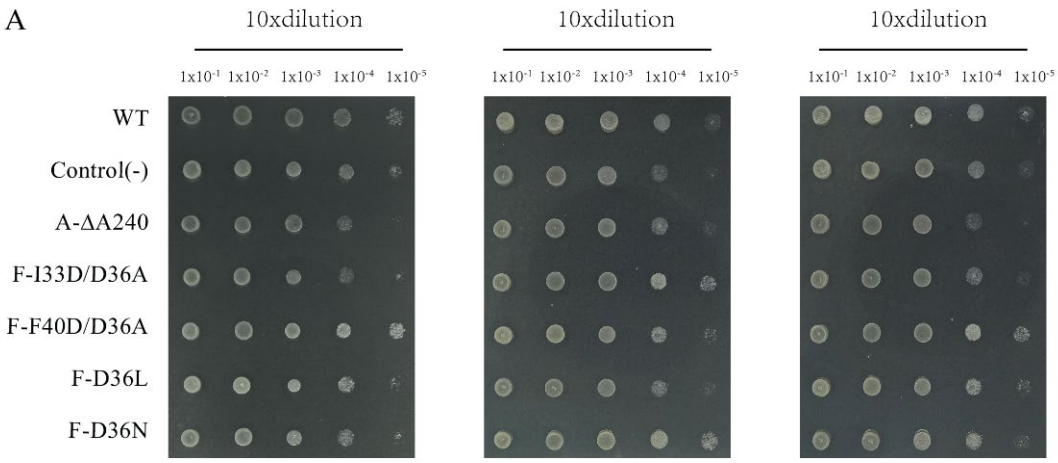

*(Fig. S7A 2/2)*

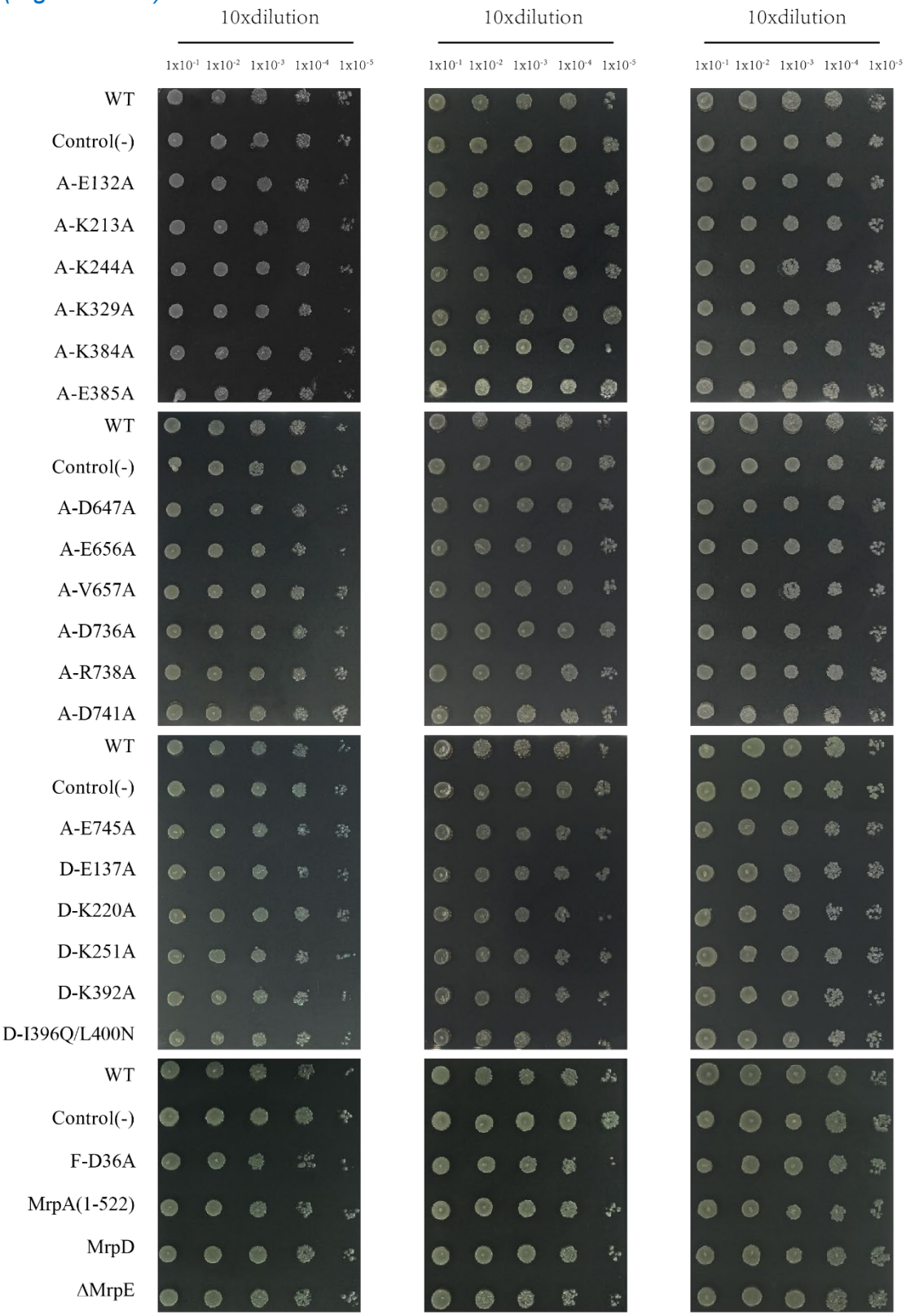
10xdilution
10xdilution
10xdilution
1x10-1 1x10-2 1x10-3 1x10-4 1x10-5
1x10-1 1x10-2 1x10-3 1x10-4 1x10-5
1x10-1 1x10-2 1x10-3 1x10-4 1x10-5
WT
Control(-)
A-E132A
A-K213A
A-K244A
A-K329A
A-K384A
A-E385A
WT
Control(-)
A-D647A
A-E656A
A-V657A
A-D736A
A-R738A
A-D741A
WT
Control(-)
A-E745A
D-E137A
D-K220A
D-K251A
D-K392A
D-I396Q/L400N
WT
Control(-)
F-D36A
MrpA(1-522)
MrpD
ΔMrpE

*(Fig. S7B)*

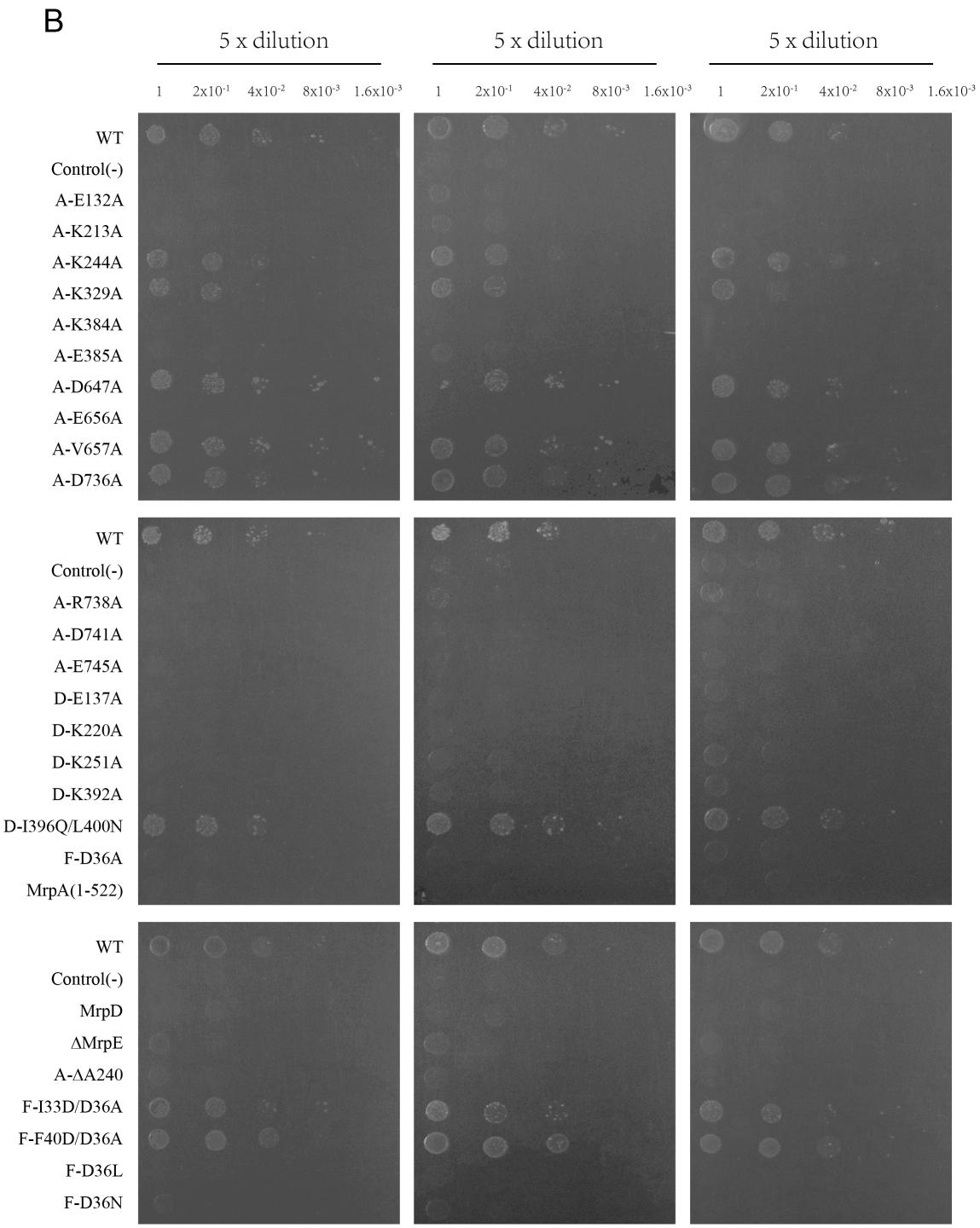
B
5 x dilution
5 x dilution
5 x dilution
1
2x10-1
4x10-2
8x10-3
1.6x10-3
WT
Control(-)
A-E132A
A-K213A
A-K244A
A-K329A
A-K384A
A-E385A
A-D647A
A-E656A
A-V657A
A-D736A
WT
Control(-)
A-R738A
A-D741A
A-E745A
D-E137A
D-K220A
D-K251A
D-K392A
D-I396Q/L400N
F-D36A
MrpA(1-522)
WT
Control(-)
MrpD
ΔMrpE
A-ΔA240
F-I33D/D36A
F-F40D/D36A
F-D36L
F-D36N

*Figure S8. Liquid salt-resistance assay in E. coli KNabc cells*

Results from negative controls at 0 M NaCl (A and E) and from assays in the presence of 200 mM NaCl (B and F) are presented. The histograms (C, D, G, H) represent cell concentrations of corresponding growth curve at plateau phase. The experiments were repeated in triplicate, each including three biological repeats. The results shown represent the mean of at least six determinations, with error bars representing std deviations. (For completeness, some data shown in Fig. 4 are repeated here.)

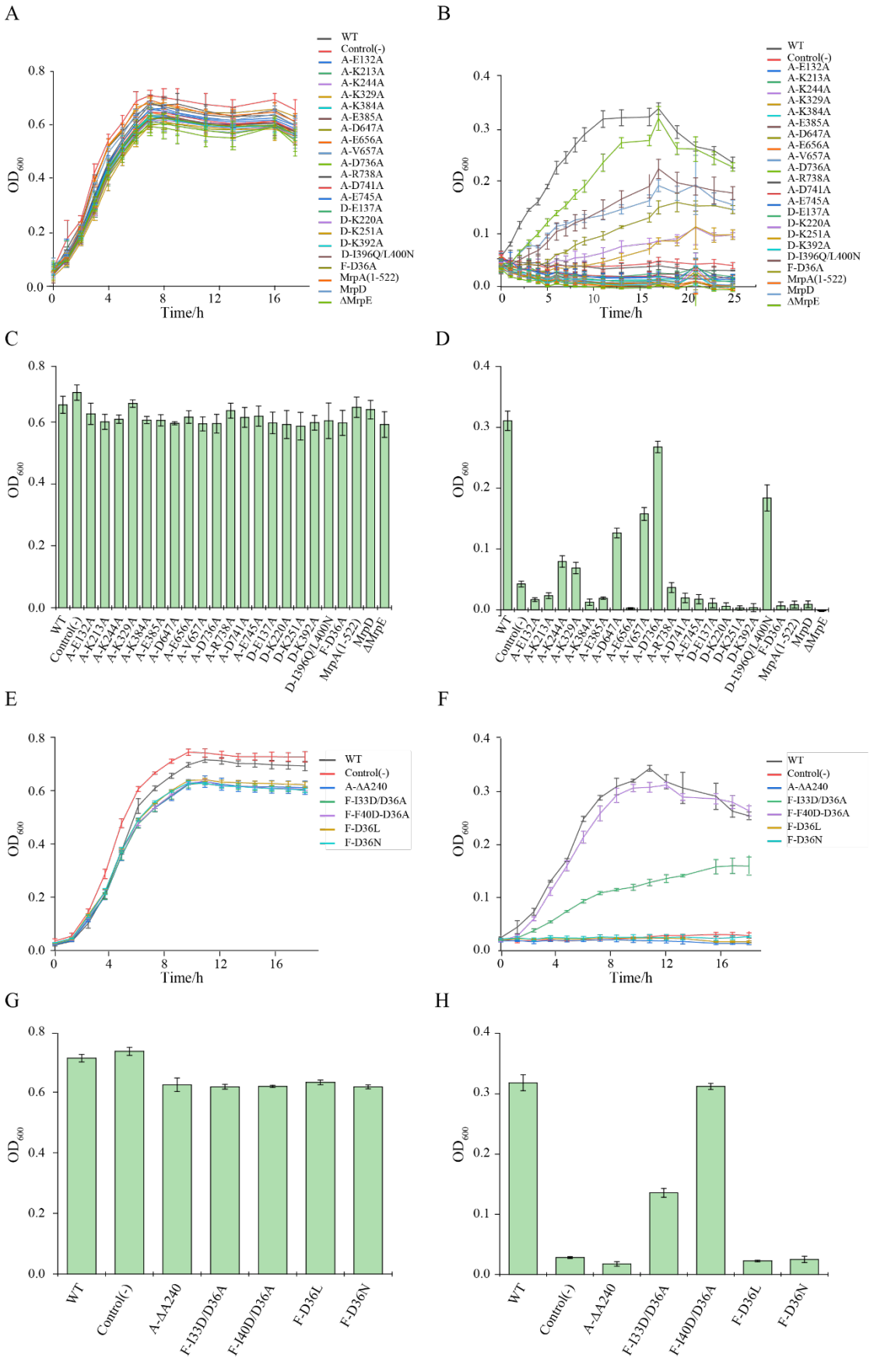
A
B
C
D
E
F
G
H
OD600
Time/h
WT
Control(-)
A-E132A
A-K213A
A-K244A
A-K329A
A-K384A
A-E385A
A-D647A
A-E656A
A-V657A
A-D736A
A-R738A
A-D741A
A-E745A
D-E137A
D-K220A
D-K251A
D-K392A
D-I396Q/L400N
F-D36A
MrpA(1-522)
MrpD
ΔMrpE
A-AA240
F-I33D/D36A
F-F40D-D36A
F-D36L
F-D36N

*Figure S9. HPLC assay of different mutants and Western Blot of individual subunits.*

(A). HPLC assay of different mutants that lost their resistance to high salt concentrations. The vertical axis represents GFP fluorescence signal. The levels of best and worst expression differed by a factor smaller than 4.

(B). SDS-PAGE of MrpA (residues 1–522 ), MrpD, and ΔMrpE, with both Coomassie Brilliant Blue stain and the fluorescence of their fused GFP.

(C). Western Blot of MrpA (residues 1–522), MrpD and ΔMrpE. The blot was probed for Strep-II tag using anti-Strep-II antibody and horseradish peroxidase-conjugated secondary antibody.

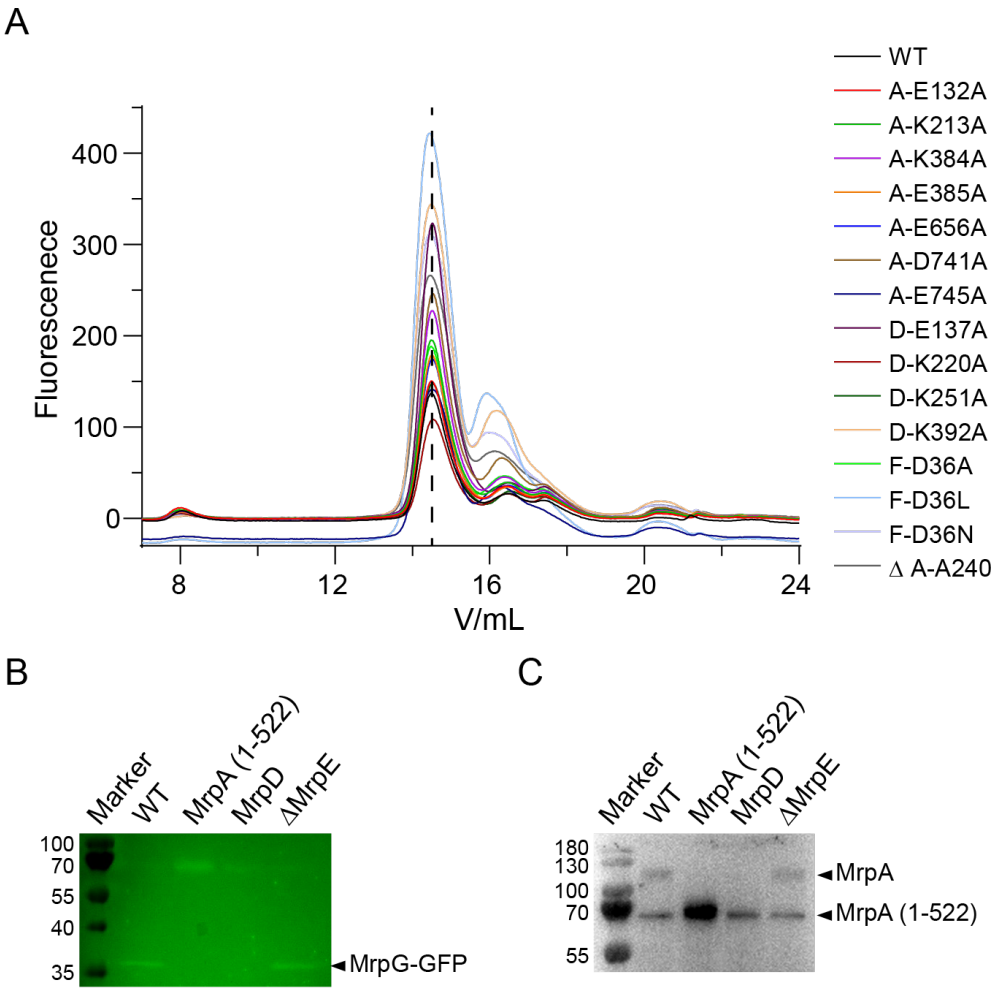

*Figure S10. Mapping of point mutations to the Mrp complex structure*

Mutations included are those from this study as well as from previous reports (1, 7, 11-13) (also see Table S2). Mutations of wild-type like behavior are depicted as green spheres; loss-of-function mutations are shown as red spheres and labeled in the side view panel; intermediates are shown as yellow spheres.

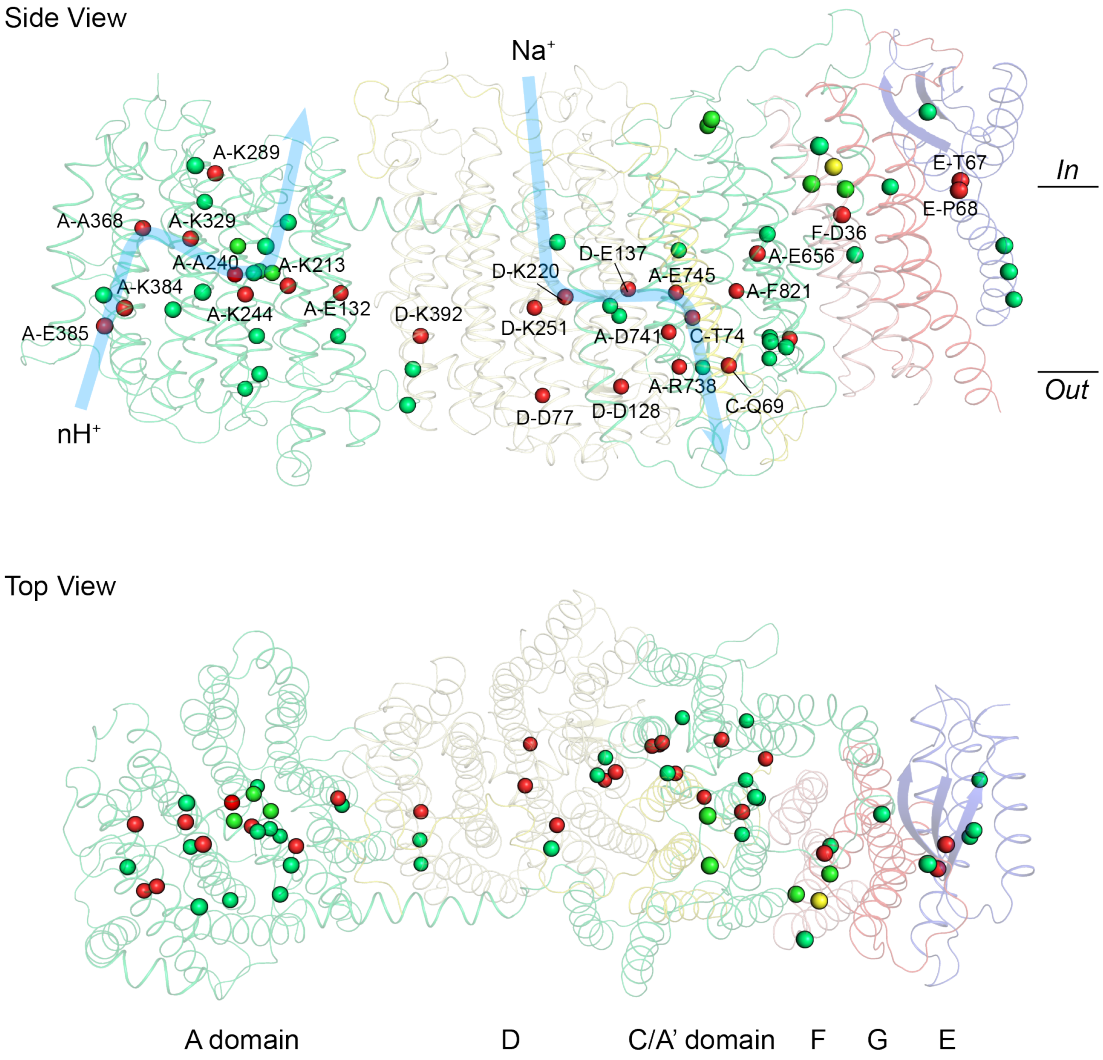

*Figure S11. Hypothetical functional cycle of the Mrp complex*

The two Mrp pumps are represented by rectangles, with other stabilizing parts (on the right side) omitted for simplicity. Substrates ($Na^+$) and driving substances (protons) are represented by magenta and cyan spheres, respectively. The dynamic connection of the central polar axis is represented by combinations of an ellipse and a (bule/red) sphere. The major point of this mechanistic model is the conformational cooperativity between subunits and competition between $Na^+$ and $nH^+$.

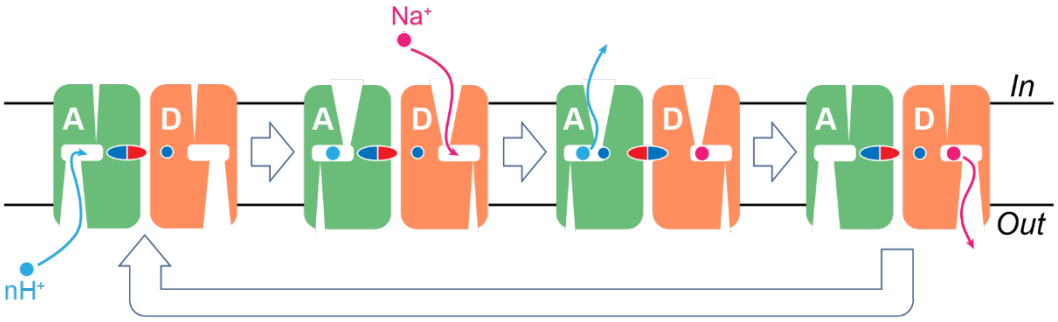

*Figure S12. Simplified energy landscape scheme of the Mrp complex*

Gibbs free-energy landscape plot describing the thermodynamic relationship between different states (8). Horizontal lines represent states; dashed lines are for hypothetical states. Ascending and descending thin arrows represent exoergic and endoergic transitions between states, respectively. Green (purple) arrows are associated with the electrostatic energy of protons ($Na^+$). Cyan (red) arrows are associated with the chemical potential of protons ($Na^+$). Subscripts L and R refer to energy terms associated with loading and releasing steps, respectively. $\Delta G_C$ is the change of conformational energy; $\Delta G_D$ [$\equiv RTln(K_{d,1}/K_{d,0})$], where subscripts 0 and 1 represent initial and final states] denotes differential binding energy of a given ligand(s). During one functional cycle, the starting and ending states are identical (*e.g.* $C_{out}H^+$ is chosen arbitrarily), only being differed by the energy dissipation (*i.e.* $Q_X$) of the Mrp complex which can be considered as the measure of the driving force. Notes: (i) Many energy terms in the plot are variable, depending on the cellular/experimental conditions, *e.g.* the membrane potential $\Delta\Psi$ and $\Delta$pH. However, in any case, the steps shown in this plot must meet the requirements of the *First* and *Second Laws* of thermodynamics. (ii) Steps marked as 'coupled' are likely to occur simultaneously.

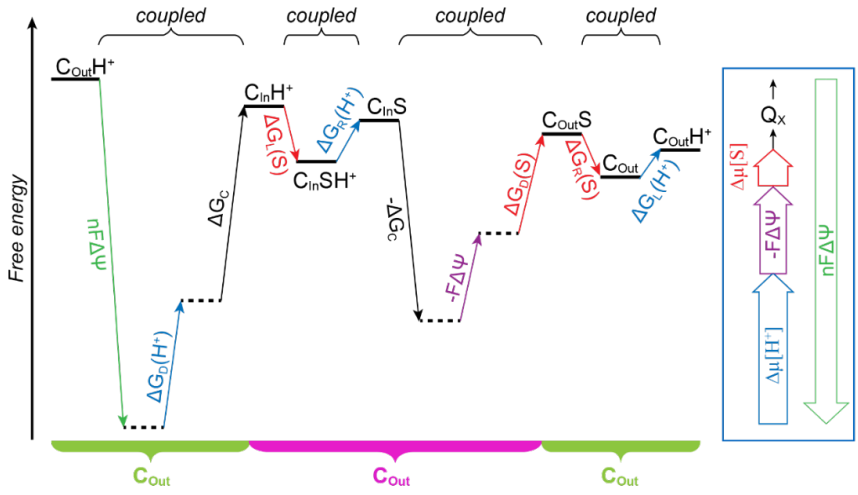

*Figure S13. Comparison of DqMrp with AfMrp*

(A). Overlay of DqMrp (green) with AfMrp (grey, PDB ID: 6Z16) shown in carton presentation (helices and ropes).

(B). The structural difference between DqMrpE and AfMrpE in the circled area of panel (A).

(C). The surface charge distribution of AfMrp. Protein surface is shown in red for negatively charged, white for neutral, and blue for positively charged area.

(D). Cavity between AfMrpA and AfMrpF in the circled area in panel (C). Lipid molecules are shown in yellow sticks.

(E). The surface charge distribution of DqMrp. Colored as in (C).

(F). The region between DqMrpA and DqMrpF as circled in panel (E) and corresponding to the AfMrpF region shown in panel (C).

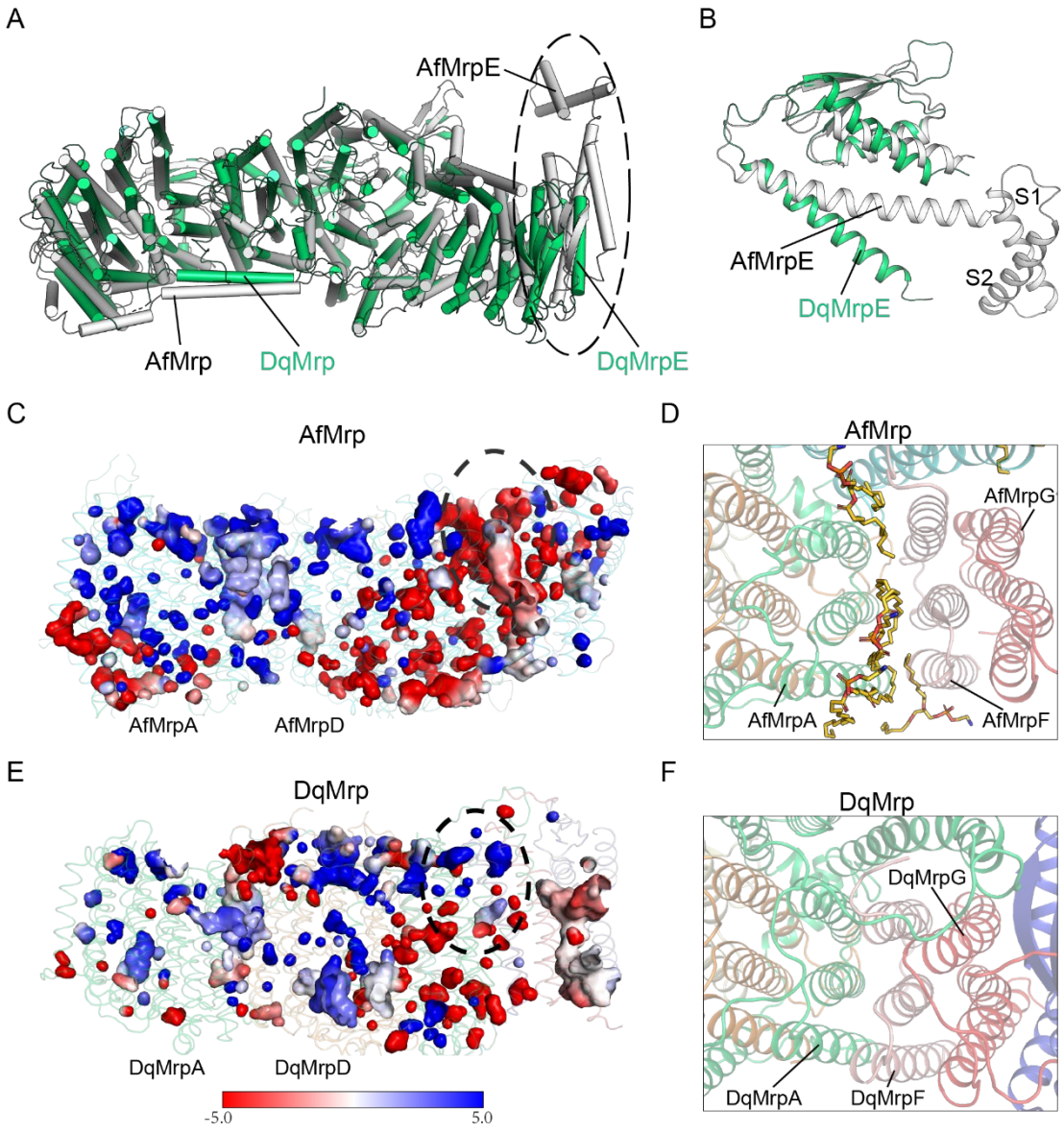
A
AfMrpE
AfMrp
DqMrp
DqMrpE
B
S1
AfMrpE
S2
DqMrpE
C
AfMrp
AfMrpA
AfMrpD
D
AfMrp
AfMrpG
AfMrpA
AfMrpF
E
DqMrp
DqMrpA
DqMrpD
-5.0
5.0
F
DqMrp
DqMrpG
DqMrpA
DqMrpF

## Supplemental Tables

*Table S1. Cryo-EM data collection, refinement and validation statistics*

| | |
|---|---|
| **Data collection** | |
| Microscope | Titan Krios |
| camera | Gatan K2 Summit |
| Magnification | 130,000 x |
| Voltage (kV) | 300 |
| Electron dose ($e^-$/ Å$^2$) | ~60 |
| Dose rate ($e^-$/pixel/s) | 10 |
| Defocus range (μm) | 1.8–2.3 |
| Pixel size | 1.04 |
| **Reconstruction** | |
| Micrographs | 1,835 |
| Particles in 3D classification | 137,082 |
| Particles in final refinement | 93,505 |
| **Refinement** | |
| Resolution (Å) | 3.0 |
| Number of atoms | 14,320 |
| Protein residues | 1872 |
| Ligands | LMT:28 |
| Sharpening B-factor (Å$^2$) | –82.30 |
| R.m.s deviations | |
| Bond lengths (Å) | 0.004 |
| Bond angles (°) | 0.591 |
| Ramachandran plot | |
| Favored (%) | 94.28 |
| Allowed (%) | 5.72 |
| Disallowed (%) | 0.00 |
| Rotamer outliers (%) | 0.50 |
| Map CC | 0.83 |
| MolProbity score | 2.14 |
| Clash score | 18.06 |

*Table S2. Summary of mutation analyses on the Mrp complex*

(Excel sheet)

## References


1. M. Morino, S. Natsui, T. H. Swartz, T. A. Krulwich, M. Ito, Single gene deletions of mrpA to mrpG and mrpE point mutations affect activity of the Mrp Na+/H+ antiporter of alkaliphilic Bacillus and formation of hetero-oligomeric Mrp complexes. *J Bacteriol* **190**, 4162-4172 (2008).
2. M. H. Saier, Jr., A functional-phylogenetic classification system for transmembrane solute transporters. *Microbiol Mol Biol Rev* **64**, 354-411 (2000).
3. T. H. Swartz, S. Ikewada, O. Ishikawa, M. Ito, T. A. Krulwich, The Mrp system: a giant among monovalent cation/proton antiporters? *Extremophiles* **9**, 345-354 (2005).
4. T. A. Krulwich, G. Sachs, E. Padan, Molecular aspects of bacterial pH sensing and homeostasis. *Nat Rev Microbiol* **9**, 330-343 (2011).
5. T. Hamamoto *et al.*, Characterization of a gene responsible for the Na+/H+ antiporter system of alkalophilic Bacillus species strain C-125. *Mol Microbiol* **14**, 939-946 (1994).
6. T. A. Krulwich, A. A. Guffanti, M. Ito, pH tolerance in Bacillus: alkaliphiles versus non-alkaliphiles. *Novartis Found Symp* **221**, 167-179; discussion 179-182 (1999).
7. M. Morino *et al.*, Single site mutations in the hetero-oligomeric Mrp antiporter from alkaliphilic Bacillus pseudofirmus OF4 that affect Na+/H+ antiport activity, sodium exclusion, individual Mrp protein levels, or Mrp complex formation. *J Biol Chem* **285**, 30942-30950 (2010).
8. X. C. Zhang, Y. Zhao, J. Heng, D. Jiang, Energy coupling mechanisms of MFS transporters. *Protein Sci* **24**, 1560-1579 (2015).
9. J. Steiner, L. Sazanov, Structure and mechanism of the Mrp complex, an ancient cation/proton antiporter. *Elife* **9** (2020).
10. F. Madeira *et al.*, The EMBL-EBI search and sequence analysis tools APIs in 2019. *Nucleic acids research* **47**, W636-W641 (2019).
11. E. Sperling, K. Gorecki, T. Drakenberg, C. Hagerhall, Functional Differentiation of Antiporter-Like Polypeptides in Complex I; a Site-Directed Mutagenesis Study of Residues Conserved in MrpA and NuoL but Not in MrpD, NuoM, and NuoN. *PLoS One* **11**, e0158972 (2016).
12. M. Morino, S. Ogoda, T. A. Krulwich, M. Ito, Differences in the

phenotypic effects of mutations in homologous MrpA and MrpD subunits of the multi-subunit Mrp-type Na(+)/H(+) antiporter. *Extremophiles* **21**, 51-64 (2017).

13. Y. Kajiyama, M. Otagiri, J. Sekiguchi, T. Kudo, S. Kosono, The MrpA, MrpB and MrpD subunits of the Mrp antiporter complex in Bacillus subtilis contain membrane-embedded and essential acidic residues. *Microbiology* **155**, 2137-2147 (2009).